HHS Public Access

Author manuscript

Sci Immunol. Author manuscript; available in PMC 2020 February 29.

Published in final edited form as:

Sci Immunol. 2019 August 30; 4(38): . doi:10.1126/sciimmunol.aaw6329.

The Position β57 of I-A^{g7} Controls the Early Anti-insulin Response and Onset of Diabetes in NOD mice to Link MHC and Disease.

Louis Gioia[2,*], **Marie Holt**[1,*], **Anne Costanzo**[1,*], **Siddhartha Sharma**[1,*], **Brian Abe**[1,7], **Lisa Kain**[1], **Maki Nakayama**[3], **Xiaoxiao Wan**[4], **Andrew Su**[2], **Clayton Mathews**[5], **Yi-Guang Chen**[6], **Emil Unanue**[4], **Luc Teyton**[1]

[1]The Scripps Research Institute, Department of Immunology and Microbiology, La Jolla, CA 92037, USA

[2]The Scripps Research Institute, Department of Integrative Structural and Computational Biology, La Jolla, CA 92037, USA

[3]University of Colorado School of Medicine, Department of Pediatrics, Department of Immunology & Microbiology, Barbara Davis Center for Diabetes, Denver. CO 80045, USA

[4]Washington University School of Medicine, Department of Pathology and Immunology, St. Louis, MO 63110, USA

[5]Medical College of Wisconsin, Department of Pediatrics, Milwaukee, WI 53226, USA

[6]University of Florida College of Medicine, Florida, Gainesville, FL 32611, USA

[7]Current affiliation: Stanford University School of Medicine, Division of Immunology & Rheumatology, Stanford, CA 94305, USA

Abstract

The class II region of the Major Histocompatibility locus is the main contributor to the genetic susceptibility to type 1 diabetes (T1D). The loss of an aspartic acid at position 57 of diabetogenic HLA-DQβ chains supports this association; it influences the recognition of peptides in the context of HLA-DQ8, and I-A^{g7} using a mechanism termed the P9 switch. Here, we built register-specific insulin MHC tetramers, Ins$_{12\text{-}20}$ and Ins$_{13\text{-}21}$, to examine anti-insulin CD4 T cell responses during the early pre-diabetic phase of disease in mice. A single cell gene expression analysis and single cell T cell receptor (TCR) sequencing of anti-insulin CD4 T cells performed in 6 and 12-week-old NOD mice, revealed tissue-specific gene expression signatures. TCR signaling and clonal expansion were found only in the islets of Langerhans. and produced either classical Th1 differentiation or an unusual Treg phenotype, independent of TCR usage. The early phase of the

Correspondence: lteyton@scripps.edu.

*Equal contribution

Author contributions: L.G., M.H., A.C., S.S. designed and performed all experiments included in the manuscript and worked as a team, B.A. performed some of the early experiments that initiated the study, L.K. was in charge of the animal colony, genotyping, and production of tetramers, N.M. provided critical DNA and cellular reagents, X.W. validated essential reagents independently of us, A.S. supervised the bioinformatics of single cell analysis, C.M and Y.C. produced the mutant mouse used in the last set of experiments, E.U. was critical in data evaluation and manuscript editing, L.T. oversaw amd coordinated the entire study and wrote the manuscript.

Conflict of interest: None of the authors have a conflict of interest with the work presented in this manuscript.

anti-insulin response was dominated by cells specific for Ins_{12-20}, the register that supports a P9 switch mode of recognition. The presence of the switch was demonstrated by TCR sequencing, re-expression, mutagenesis, and functional testing of αβ TCR pairs in vitro. The genetic correction of the β57 mutation resulted in the disappearance of D/E residues in the CDR3β of anti-Ins_{12-20} T cells, and inability of cells normally activated by a switch to recognize the Ins_{9-23} peptide. These results provide the first molecular mechanistic explanation that links the unique MHC class II polymorphism of T1D with the recognition of islet antigens and disease onset.

Introduction

The association between HLA genes and autoimmune diseases was uncovered more than 40 years ago(1). Among them was type 1 diabetes(2) (T1D) and a linkage to HLA-DR3 and -DR4 that explained the vast majority of the genetic component of this serious disease(3, 4) in which the exclusive destruction of the β cells of the islets of Langerhans of the endocrine pancreas leads to a lifelong dependency on insulin replacement therapy. The linkage to two HLA-DR haplotypes was later redefined as an association with the HLA-DQ haplotypes that segregate with these HLA-DR genes, HLA-DQ2 and HLA-DQ8 for HLA-DR3 and HLA-DR4, respectively. Relative risk is higher for HLA-DQ2 and HLA-DQ8 homozygotes than for heterozygotes, and maximal for HLA-DQ2/HLA-DQ8 heterozygotes(5). In 1987, McDevitt's group made the important observation that every HLA class II associated to T1D was carrying a distinct polymorphism at position 57 of the β chain that substituted the normal aspartic acid of all MHC class II β chains at this position by a neutral residue(6). This striking observation has been confirmed since in one of the largest genetic study of T1D(7). Structurally speaking, the consequences of this alteration are the loss of a salt bridge with the arginine 76 of the α chain and the appearance of a surface-exposed positively charged patch that modifies both the P9 pocket and potential TCR contacts(8, 9). We, and others, have shown that the loss of the salt bridge had no consequence on the structural integrity of the molecule(8, 10) and that it remained stable and competent for peptide binding. As expected, the modifications of surface charges at the P9 pocket impact peptide binding profoundly, and the peptide repertoire of diabetogenic MHC class II molecules is heavily biased towards the selection of peptides with acidic residues at P9(11, 12). However, like most I-A and HLA-DQ molecules, diabetogenic MHC class II proteins remain very promiscuous for peptide binding as they interact mainly with the peptide backbone instead of using anchor residues(13, 14). The consequence of this mode of binding is that all MHC class II molecules without Aspβ57 can also bind efficiently peptides that do not have a negatively charged residue at the P9 position(8, 14). In this case, a large positively charged patch remains surface exposed and potentially accessible to T cell recognition. We have evaluated this situation by immunizing NOD mice and HLA-DQ8 transgenic NOD mice with peptides carrying or not a negatively charged residue at the P9 position. In both instances, we have shown that the absence of charge at that position in the peptide resulted in the selection of T cell receptors (TCRs) that encoded either an Asp or a Glu residue at position P+2 or P+3 of their complementary determining region 3β (CDR3 β)(9, 15). For one of those peptides derived from hen egg lysozyme that has a glycine at P9, we also demonstrated biophysically and structurally that the presence of a negatively charged residue at position 2 or 3 of the CDR3β increased the affinity of the TCR for its cognate peptide-

MHC complex by more than thirty fold(9). We called this mode of TCR recognition the “P9 switch” and suggested that it might be important in the initiation of diseases such as celiac sprue and T1D which are tightly associated to non-Aspβ57 MHC class II molecules. However, in the absence of important reagents such as appropriate MHC tetramers and/or animal models, e.g. celiac disease mouse model, we could not formerly test our hypothesis. The development of I-A^{g7} tetramers capable of distinguishing the two main registers of the $insulin_{9\text{-}23}$ peptide(16) was the first important step in testing the relevance of the P9 switch model in T1D because one of them, $Ins_{12\text{-}20}$, has a glycine at P9 whereas the other one, $Ins_{13\text{-}21}$, bears a glutamic acid at that position. Recognition of insulin requires its processing in intracellular compartments of the presenting cells resulting in the presentation of the $Ins_{13\text{-}21}$ peptide segment. T cells that recognize the $Ins_{13\text{-}21}$ peptide either from such processing of insulin or from exogenous peptides, represent the conventional presentation-type A cells. In contrast, other peptide segments, like $Ins_{12\text{-}20}$, are eliminated by the intracellular processing of insulin and are normally not presented. Importantly, the $Ins_{12\text{-}20}$ peptide segment can be presented from exogenous peptides and recognized by T cells- type B cells. This mode of presentation takes place when beta cell crinosomes partially catabolize insulin molecules and release a number of insulin peptides which are then presented in islets as well as in peripheral lymph nodes (17).

In any instance, if the P9 switch model were correct, one would expect three simultaneous findings: 1) $CD4^+$ T cells restricted on pMHC with neutral P9 residues should be preferentially expanded, 2) The same cells should be activated earlier than cells recognizing pMHC with Asp/Glu at P9, 3) These cells should rely on Coulombic forces for interaction. We have already shown that cells specific for a BDC2.5 mimotope with a neutral P9 position were preferentially expanded in the NOD mouse and that those cells had higher affinity for their pMHC than cells specific for BDC2.5 peptides with Asp at the P9 position(9). We now demonstrate that the nature of the amino acid at position β57 controls the selection and expansion of CD4 T cells specific for insulin and the onset of T1D in the mouse. Using single CD4 T cell analysis, we show that the tissue of origin of anti-insulin T cells could easily be identified based on unique gene expression signatures. Stigma of TCR signaling and T cell expansion appeared to be localized exclusively to the islet rather than the pancreatic lymph node. While islet-infiltrating T cells were either classic T_{H1} or Treg cells, this dichotomy was not associated to particular TCRαβ pairs.

The early T cell response seen in the islets was dominated by anti-$Ins_{12\text{-}20}$ cells. A majority of these cells carried a Asp/Glu (D/E) residue in their CDR3β and used a switch for recognition. The restitution of an aspartic acid at position β57 of I-A^{g7} in vivo, eliminated this population of cells.

These results provide the first mechanistic molecular explanation why and how diabetogenic MHC class II molecules increase the risk of autoimmunity.

Results

MHC class II tetramers specific of the two registers of insulin$_{9-23}$.

The expression of functional MHC class II tetramers remains difficult especially when multiple registers can be displayed within short peptides. The length and nature of the linker when expressing tethered peptides, the on and off rates of the peptides itself, and the potential role of flanking residues are all factors to consider when expressing MHC class II-peptide complexes. In addition, in many instances expression does not mean proper display as many recombinant MHC class II molecules are unable to activate and/or bind T cells that are specific for the cognate peptide(18). We have successfully expressed the various registers of ovalbumin in I-A^d and I-A^b by using a short seven residue linker(19) but failed to express functional Ins$_{12-20}$ and Ins$_{13-21}$ peptides in I-A^{g7} using the same approach. The re-engineering of both peptide and MHC to introduce artificial disulfide bridges as proposed by some(20, 21), led to expression of non-functional molecules (that is, no stimulation of T cell hybridomas and no T cell staining ex vivo, our data, not shown). We then applied various modifications at anchor residues or N and C-terminal flanking residues (P-1 and P10) with the idea to limit register sliding or inadequate display; none was successful (Supplementary table 1). Finally, we explored the ability of various sequences such as poly-glycine stretches to disrupt type II polyproline helices(22), the normal required secondary structure of peptides for binding to MHC class II molecules. The addition of three C-terminal glycines allowed the expression of Ins$_{13-21}$, whereas the addition of four allowed the expression of both Ins$_{12-20}$ and Ins$_{13-21}$. The specificity and functionality of the recombinant molecules were tested by staining and stimulating T cell clones specific for each register (Figure 1). Accordingly, type A cells of which IIT3 is a representative(23) were stained and stimulated specifically by recombinant I-A^{g7}Ins$_{13-21}$ molecules, whereas type B cell such as 2D10 were stained and responsive to I-A^{g7}Ins$_{12-20}$ molecules.

Ex vivo detection of insulin-reactive CD4$^+$ T ceils in naïve NOD mice.

Following this characterization, the MHC tetramers were tested ex vivo to quantify the CD4$^+$ T cells from thymus, spleen, pancreatic lymph nodes, and islet infiltration from NOD mice of different ages. The specificity of the reagents and the existence of two distinct populations of cells was confirmed by double staining (Figure 1A, B). In all cases, insulin-reactive cells were detected in the thymus and peripheral lymph nodes; consistently Ins$_{12-20}$ cells were twice as numerous as Ins$_{13-21}$ cells in pre-diabetic mice while both populations, at difference with BDC2.5 cells(24), showed no significant expansion between thymus and PLN (Figure 1C). However, in the islets at 6 weeks of age, the Ins$_{12-20}$ cells showed a 200 to 400 fold expansion which contributed to most of the infiltrating CD4 population of a majority of mice (Figure 2A, B, C). The Ins$_{13-21}$ cells while also more numerous in the islets than in PLNs, never represented more than 20% of the infiltrating CD4 population and a pairwise analysis of each mouse showed that Ins$_{12-20}$ cells dominated the early phase of autoimmunity (Figure 2C). Across all 6 week-old mice (n=11), the mean representation of Ins$_{12-20}$-specific cells in the islets was 52.05% of all CD4 T cells (with a SEM of 8.0%), while Ins$_{13-21}$-specific cells had a mean representation of 11.26% (with a SEM of 1.96%), establishing the high significant difference of frequencies between the two populations ($p<0.0001$). Interestingly, numbers dropped to 3.31% (SEM=1.42%), and 1.65%

(SEM=0.82%) for Ins_{12-20} and Ins_{13-21}-specific cells, respectively, at 12 weeks of age, with no statistical difference of representation of either population (p=0.352). These results indicated the likely importance of the P9-switch for early pathology but not for progression. This conclusion was reinforced by examining the anti-insulin response in overtly diabetic mice, and seeing the same disappearance of the differential between the two populations with no statistical differences in both spleen (p=0.68) and PLNs (p=0.15) (Figure 2D).

Single cell expression profiling of insulin-reactive CD4$^+$ T cells reveals organ residence signature and key steps of pathogenesis.

Having appropriate reagents, anti-insulin register-specific T cells were sorted by cytometry as single cells in 96-well plates using a dump negative (CD8-B220-CD11b)-CD3+CD4+tetramer+ gate. Each cell was examined for the expression of a set of 96 genes surveying surface receptors, cytokines, signaling molecules, chemokines and chemokine receptors, transcription factors, and cytokine response genes(25). Profiles were established from individual 6-week and 12-weeks old mice, and based on the analysis of 1580 individual cells of which 501 were from islets, 729 were from PLNs, and 350 from the spleen.; 967 cells were from 6-week-old (n=11) and 613 cells from 12-week-old mice (n=4). With or without GAPDH normalization, unsupervised clustering could define six subsets. However, as illustrated in Figure 3A, 1060 cells, besides CD3, CD4, and housekeeping genes, were expressing less than 10 of the 96 chosen genes at detectable levels and needed to be removed from further statistical analysis to evaluate the differential expression between cells expressing large number of genes. Accordingly, 87.2% of cells from the spleen, 66.4% from the PLN, and 54% from the islet were removed from the unsupervised cluster analysis (Figure 3B). In spleen and PLNs, these numbers correlated with the recently described phenotype of functional anergy defined as FR4+ - CD73+ in the CD44+ population: (Supplementary Figure S1)(26). Following this curation, the unsupervised clustering revealed four different groups (Figure 3C, D, and Supplementary Figure S2). This cluster definition was not influenced by age (6 versus 12 weeks), or the reactivity of the cell (Ins_{12-20} versus Ins_{13-21}). Cells from cluster #1 were represented in all three tissues and, besides CD3 and CD4, expressed genes associated with cell adhesion and sustained activation of T cells, CD86, ICAM1, CD80, CD40(27, 28), as well as two transcription factors, Zeb2 and PPARγ, involved in terminal differentiation and effector function of T cells(29). This cluster of cells was the only one that increased significantly between 6 and 12 weeks. Cluster #2 was over-represented in PLNs and notable by absent features: no signs of TCR- or cytokine mediated signaling, no markers associated with the major CD4 subsets. CCR7, a chemokine receptor strongly linked to lymph node homing was the highest expressed gene in this cluster (Table 1). Clusters #3 and #4 identified the cells resident of islets, and a very small percentage of PLN cells (Figure 3). Cluster #3 cells were prototypic Th1 cells with high expression of Th1 cytokines such as IFNγ, TNFα, and IL-21, TCR-triggered signaling molecules such as CD3, Zap-70, and Fyn, and high expression of co-activator genes including CD28 and ICOS. The expression of IFNγ and TNFα was confirmed by flow cytometry for the whole intra-islet CD4 T cell population, and very few cells were found to be double expressors (Figure S3). Cluster #4 was more intriguing with high expression of typical Treg-associated genes, Foxp3, IL2Rα, and IL-10, but also persistent expression of T-bet, and in some cells IFNγ and TNFα (Figure 3E). The presence

of Foxp3+CD25+ was detected by flow cytometry at increased frequency in infiltrated islets compared to peripheral lymphoid tissues for both Ins_{12-20} and Ins_{13-21}-specific cells (Figure S4). The overlap of high gene expression between Clusters #3 and #4 shared PD1, CTLA4, ICOS, and TCR signaling molecules, Zap70, Fyn, and Nur77 (Table 1 and Figure 3E); we interpreted this overlap as a stigma of the possible transition between the two subsets, indicative of the plasticity of T cells. In any instance, the near equal representation of the two clusters, 45.6% of cells in cluster #3, 34.5% in cluster #4 (Figure 3D), in the entire anti-insulin T cell population regardless of register usage, indicated that antigen alone was not the determinant factor for effector function.

We conclude from the single cell gene analysis that the intra-islet events determine much of the final fate of the T cells, regardless of their specificity.

TCR sequencing of insulin-reactive $CD4^+$ T cells: Confirmation of the P9 switch model and islet pauciclonal expansion.

Single cell TCR sequencing of tetramer sorted T cells was carried out using the same reaction used for RNA expression profiling(25). Briefly, following a pre-amplification step, a second round of PCR was used to amplify and bar code each cell with a common tag on the Cα and Cβ primers. The final library was produced by using a nested PCR approach with internal Cα and Cβ primers and analyzed on a Miseq next generation sequencer(25). It is important to mention that the efficiency of sequencing of TCR chains was highly dependent on the state of activation of the cell as measured on our 96 genes set; chain pairing was successful in ~70% of cases while in the remaining 30% only one of the two TCR chains could be sequenced. In the absence of upregulation of at least 50% of the 96 genes that we evaluated in our panel, TCR sequencing efficiency was always low (<20%). Consequently, very few sequences were recovered from spleen, and fewer from PLNs than from islets. The first information that came from this analysis is that both Ins_{12-20} and Ins_{13-21} cells in PLN and islets expressed diverse TRAV and TRBV segments with slightly more diversity in the islets (Figure 4). This diversity came with some bias and an over-representation of TRAV6.5, 6.6, and 5D4, and TRBV2, 5, and 13.1 for Ins_{12-20} cells in both locations, while TRBV1, 5, and 13.2 were over-represented for Ins_{13-21} cells in the islets. The profiles of Ins_{12-20} V segments usage, although very similar between islets and PLN, did not correspond to matching TCR pairs in the two locations; similarly, no identical TCRs could be found between mice. A pairwise analysis (Figure 4B) revealed some preferential Vα/Vβ pairing for Ins_{12-20} cells but all of these pairs corresponded to clones. As we defined the occurrence of clonal expansion by the sequencing of the same TCR pair in 3 or more cells in the same location, clones were only detected in islets and never in PLNs, and most were found at 6 week of age and were specific for Ins_{12-20} (Figures 4B, 5A). Importantly when cluster identity was examined for each clone, while most of them belonged to either cluster #3 or #4, some were split between clusters (Figure 5A). These observations, strongly supported the hypothesis that antigen recognition and expansion took place in the islets and not the lymph node, and demonstrated that the functional fate, Th1 versus Treg, was not exclusively dependent on TCR usage. To support the first conclusion, Ins_{12-20} and Ins_{13-21} T cell hybridomas were stimulated with fresh islets cells and PLN cells in the absence of

exogenous peptides. As seen in Figure 5B, only islet cells activated Ins-specific clones while PLN cells, even in much larger numbers did not (Figure 5B).

Besides measuring length at ~14.0+/−1.0 amino acids for both α and β, the examination of the CDR3 regions of TCRs isolated from islet and PLN revealed the increased frequency of negatively-charged residues at position +3 of CDR3β of $Ins_{12\text{-}20}$ T cells, suggesting the existence of a P9 switch (Figure 6A). In most cases, this D/E residue was encoded by a non-germline sequence, indicating the role of the antigen recognition in the selection and expansion of these populations (Supplementary List 1). To confirm the functionality of this switch, three TCR α-β pairs isolated from islet cells and retaining a negative charge in CDR3β, were cloned and re-expressed in BW-5147 TCR negative cells using the lentiviral vector pMIG2(30), and used for functional test on plastic bound pMHC molecules. Beyond confirming specificity for $Ins_{12\text{-}20}$, the titration of ligand demonstrated that the functional avidity of the three TCR pairs varied substantially with stimulatory index 50 (SI_{50}) comprised between 60 and 200ng of ligand per well (Figure 6B). More importantly, the confrontation of these clones to an I-A^{g7} $Ins_{12\text{-}20}$ complex mutated at position 9 of the peptide for a glutamic acid ($Ins_{12\text{-}20}$ P9E) resulted in the complete absence of stimulation (Figure 6B). The same result was obtained for 2D10 and 8F10 T cells, two T cells isolated from immunized mice, and whose SI_{50} are 5 and 50 ng of ligand per well, respectively (Figure 6C). The reciprocal experiment was performed by mutating the glutamic acid residue 114 in the CDR3β of Cl2 TCR and testing both WT and mutant TCRs on I-A^{g7} $Ins_{12\text{-}20}$ complex (Figure 6D); the mutant Cl2 T cells was unresponsive. Finally, the same experiment was performed using recombinant 2D10 TCR and its $CDR3\beta_{116}$D➔G mutant using plasmon resonance for affinity measurements (Figure 6E). Both WT and mutant TCRs were captured at the surface of a lipid bilayer by their C-terminal histidine tails using a DOGS lipid and tested for binding to I-A^{g7} $Ins_{12\text{-}20}$. As shown in the figure, while the WT 2D10 TCR bound with measurable affinity ($K_{ass}=1.9\times10^{4}M.s^{-1}$, $K_{diss}= 0.01s^{-1}$, $K_d=4.44\times10^{-7}$), the point mutation resulted in an almost complete loss of measurable binding (association rate was not quantifiable), confirming the functionality of the switch in this TCR.

Genetic demonstration of the role of the switch in insulin recognition.

The importance of mutations at position β56 and β57 of I-A^{g7} in the onset of insulitis and diabetes, was tested 25 years ago by transgenesis in the NOD mouse using $A\beta^{k}$ and $A\beta^{d}$ transgenes(31–34). The more focused targeting of position I-A^{g7}β57Ser➔Asp was also tested by transgenesis and resulted in a marked reduction in diabetes but a persistence of peri-insulitis(35, 36). These transgenic mouse models were very imperfect, mainly because they all still carried a normal I-A^{g7} molecule. Indeed, we showed that the simple dilution of a WT IA^{g7} into a NOD-$A^{0/0}$ background (NOD-$A^{0/0}$ x NOD F1 mouse) was sufficient to prevent diabetes, establishing that the quantity of MHC and or antigen displayed by MHC on antigen presenting cells was controlling disease onset (Figure S5). Because of these limitations, none of the transgenic experiments could address the mechanisms by which position β57 altered T cell responses and progression towards autoimmunity. To access this information directly, the serine β57 of I-A^{g7} was mutated to an aspartic acid using zinc-finger nuclease (ZFN) technology directly in NOD mice(37). Before examination, the new

mouse line was backcrossed twice into the WT NOD background to eliminate any potential off-target effect of ZFN cleavage and repair. Neither males, nor females of this mutant mouse line developed diabetes and no periinsulitis could be observed in mice, even after 20 weeks. Mutant I-$A^{g7}S_{57}$➔D tetramers were recombinantly expressed for both insulin peptides, and used to quantify anti-insulin CD4 T cells in the mutant mouse. As shown in Figure 7, in thymus, spleen and PLNs of 8-week old female mice, numbers of $Ins_{12\text{-}20}$ and $Ins_{13\text{-}21}$ T cells were equivalent ($p=0.07$ in spleen, $p=0.29$ in PLNs, and 0.13 in thymus); numbers could not be obtained from islets since so few CD4 T cells could be isolated. It is noteworthy to mention that while tetramer+ cells were in almost identical numbers in the spleen of the mutant mouse as in WT mice, numbers in PLNs were three times lower in the β57 mutant animal (Figures 1, 7). The TCRs of the rare insulin-specific cells isolated from this location (PLNs) were sequenced and compared to WT PLNs TCR sequences (Figure 7B). The disappearance of D/E residues in CDR3β of $Ins_{12\text{-}20}$-specific T cells from mutant animals as compared to WT mice was highly significant (13.3% versus 28.2%, $p<0.001$), confirming the direct role of serine β57 in the selection of this particular TCR repertoire. The influence of β57 was also shown functionally by comparing the presentation of hen egg lysozyme (HEL) and insulin by antigen presenting cells from WT or mutant mice. As shown in Figure 7C, the presentation of HEL was diminished when the antigen was presented to the anti-HEL TCR 21.30 by mutant as compared to presenting cells from regular NOD mice, confirming our previous studies(9), while the recognition of the $Ins_{9\text{-}23}$ peptide was completely abbrogated for all $Ins_{12\text{-}20}$-specific T cells that we tested and of which clone 9 is a representative. Presentation of $Ins_{9\text{-}23}$ peptide to the prototypic anti-Ins13-21 11T3 T cell hybridoma was nearly identical between NOD and β57 mutant mice (Figure S6).

Discussion

The development of reagents that could detect selectively the two main adjacent registers of the $insulin_{9\text{-}23}$ peptide allowed us to dissect some fundamental aspects of the biology of I-A^{g7} molecules and their impact in the pathogeny of T1D. Beyond showing the importance of peptide registers in the biology of I-A and HLA-DQ molecules(15, 19, 38), these new tetramers confirmed the existence of two adjacent registers in the $B_{9\text{-}23}$ segment of insulin(16, 39).

The interrogation of the biology of autoreactive T cells against a nominal antigen using single cell analysis and a set of selected T cell-related genes revealed some important aspects of autoimmunity. Foremost, the fact that a majority of anti-insulin T cells were expressing very low levels of any of the 96 genes that we selected as indicators of T cell functions, in the spleen, lymph nodes, and even islets seems to correlate well with the strong state of peripheral anergy towards insulin that is observed in most mouse genetic backgrounds, including the NOD mouse. This “anergy” was also correlated phenotypically with the expression of CD73 and FR4 in the CD44+ population(26). Functionally, this overall concept of “high degree of tolerance towards insulin” is confirmed by the outcome of immunization of mice with $B_{9\text{-}23}$ peptide or insulin; in our hands, and in publications, it seems that insulin administration rarely produces measurable CD4 T cell expansion, regardless of the adjuvant used, although it induces cytokine secretion measurable by ELISPOT(23, 40). Recent studies indicate that there is a continuous and low levels of

presentation of insulin peptides in all peripheral lymph nodes including the pancreatic nodes. The peptides are derived from crinosomes released into the circulation following a glucose challenge. This low level and persistent presentation in peripheral nodes induced in the 8F10 T cells that recognize $Ins_{12\text{-}20}$ a level of activation but not anergy. It is noteworthy that ablation of lymph node results in complete absence of diabetes and T cell priming(41). This response at the periphery will likely vary among T cells depending on their TCR specificities and affinities. Regardless the islet presentation will profoundly influence the response based on its display of a number of regulatory molecules such as PD1. Therefore, it seems logical that tolerance to insulin will have a higher chance of being broken in the environment of the islet where all forms of insulin and its by- and abortive products are presented. Studies in TCR transgenic mice have supported this hypothesis(39), and our gene expression and T cell repertoire analyses of insulin-specific cells strongly supported the same conclusion. What allows the breakage of tolerance in the islets? Is it linked to antigen processing and presentation? The effects of the dilution of $I\text{-}A^{g7}$ in MHC knockout NOD mice demonstrates this is likely the case. But, besides the existence of a threshold for the quantities of particular peptide-MHC complexes needed to activate autoreactive cells, the classical model of T cell activation tells us that effective costimulation as well as a milieu providing cytokines and growth factors(42) will be necessary. In an inflammatory context, it appears that the islet resident macrophage is the most likely cell responsible for self-antigen presentation. Not only do they capture immunogenic peptides from the crinophagic granules upon insulin stimulation(17), but they express a very efficient antigen processing and presentation machinery(43), and their elimination results in the prevention of disease(44). Of course, it cannot be completely ruled out that in the context of the islet, beta cells themselves contribute to T cell stimulation as they have been shown to express MHC class I and II upon TNF-IFNγ stimulation(45), two cytokines that are found in the lesion. A two cell types presentation scenario might explain one of the most surprising finding of our study: the ability of T cell clones to differentiate either as Th1 or Treg cells (Figure 5A). For instance, the engagement of PD1 by the PDL1 expressed by beta cells might favor Treg over Th1 differentiation(46). Additionally, the ability for a single T cell to receive signals from two presenting cells might also explain the persistence of Th1 stigma such as Tbx21, and IFNγ, in some Treg cells(47, 48). It is also important to contrast findings in the islets and the PLNs, a location where we never found clonal expansion, and in which Tregs did not express Tbx21 in addition to Foxp3, and presented only the classical features of the family, suggesting that Tregs were receiving additional differentiation signals in the islets.

The second most important conclusion of our study is the demonstration of the critical role that the P9 switch mode of recognition plays in the pathogeny of T1D, as illustrated with the $Ins_{12\text{-}20}$ peptide. If the P5 position of that peptide has been shown to be essential for diabetes development(49), we show here that the P9 switch is essential for the function of $Ins_{12\text{-}20}$-specific T cells and that at the population level a D/E residue in CDR3β is selected and necessary for T cell recognition. Examination of infiltrating CD4 T cells at 6 weeks of age when insulitis is minimal, also demonstrated the preferential expansion of $Ins_{12\text{-}20}$-specific T cells at the early pre-clinical phase of disease, indicating the proliferative advantage that the P9 switch provides to T cells. It is quite remarkable to see that more than 50% of the CD4 islet infiltrate is made of these cells at 6 weeks. It will be of upmost interest to determine

whether the remaining cells also use a switch for recognition and expansion, and if peptides are provided by other fragments of insulin. Particular attention will be given to the C-peptide, a major source of antigen in man(50) and mice(51, 52); indeed, almost all human C-peptide derived epitopes(50), as well as the immunodominant murine C-peptide determinant(51) have no negative charge at P9. In human, the recognition of these peptides by TCRs fulfilling the canons of a P9 switch mode of T cell recognition with D/E amino acids in their CDR3β has already been reported(53). In mice, similar observations were made for non-insulin epitopes devoid of D/E P9 residues(9).

Finally, the kinetics of the P9 switch-driven anti-insulin response in mice with its early burst and rapid disappearance, have important translational implications. Indeed, if they also exist in man, it is only in at-risk patients that these cells would be detectable; their capture from peripheral blood could constitute the earliest possible marker of islet autoimmunity, and change the timing of therapeutic intervention.

Our observations regarding the potential role of the P9 switch mode of T cell recognition in the onset of diabetes in the NOD mouse were challenged by the examination of the mutant β57 S➔D mouse. Our predicition was that the disappearance of the positively charge surface at P9 would eliminate T cells capable of using the P9 switch. As a result, $Ins_{12\text{-}20}$ peptide should select a normal T cell repertoire without D/E residues in the N-terminal segment of the CDR3β. While this expectation was proven correct by direct sequencing of the anti-$Ins_{12\text{-}20}$ TCRs, the enumeration of anti-insulin cells showed their marked reduction in PLNs as compared to WT NOD mice and their near complete elimination in the islet. This latest point established the direct role of P9 switch cells in the initiation of infiltration and the inability of cells without switch to substitute for them. Therefore, the binding advantage that we have documented for P9 switch cells appears necessary and sufficient to break tolerance in the context of islet antigen presentation. This simple relationship between position β57 of diabetogenic MHC molecules and the selection of a unique T cell repertoire appears to be the molecular mechanism that links MHC and T1D. Further studies will attempt to confirm this conclusion in man. This task might prove challenging since while the switch plays an essential role in initiation, it appears not necessary for continuation of disease. However, the examination of at-risk, and just-diagnosed patients should allow us to overcome this difficulty. The initial analysis of anti-C-peptide CD4 T cells that showed the presence of D/E residues in CDR3β makes us optimistic(53).

Finally, it is likely that antibodies or small molecules capable of interfering with the position β57 of HLA-DQ8, if applied early enough in the development of the autoimmune process, would be capable of preventing progression and onset of disease.

Material and Methods

Mice.

NOD/LtJ mice were purchased from Jackson Laboratories and housed in pathogen-free conditions. Care and handling followed institutional IACUC rules. Glycemia of all animals was measured weekly from a drop of blood collected from the tip of tail.

Cells and transfection.

BW5147 ($TCR^{\alpha-\beta-}$) cells and T cell hybridomas were maintained in DMEM-10% FCS medium. For re-expression of TCR in BW5147, after sequencing Vα and Vβ segments were synthesized and cloned into pMIG II (Addgene*) and spinfected with polybrene for 2h at room temperature at 1,000g(30). After recovery, cell expressing TCR were sorted by staining with the anti-TCRb chain antibody H57-597 (BD Bioscience*)

Construction, Expression and Purification of I-A^{g7}/Peptide and recombinant TCR Molecules. Generation of Tetrameric MHC Molecules.

The generation of I-A^{g7}/peptide complexes has previously been reported in detail(54). The peptide sequences of I-$A^{g7}$$HEL_{11-27}$, I-$A^{g7}$$Ins_{12-20}$, and I-$A^{g7}$$Ins_{13-21}$ molecules are AMKRHGLDNYRGYSLGN, VEALYLVCG, and EALYLVCGE, respectively. The biotinylation sequence #85 from Schatz follows the acidic zipper on the α chain. Biotinylation was performed in vivo by cotransfecting an inducible BirA plasmid, and adding 50μM biotin at the time of induction. After purification by ion exchange and size exclusion, biotinylated molecules were tetramerized at 4°C overnight using PE-labeled (BioSource International*) or PE-Cyanine 7, or APC-labeled streptavidin (eBioscience*) using a 5:1 molar ratio of biotinylated molecules to labeled streptavidin.

For SPR measurements on lipid bilayers, the same pMHC molecules were produced with a C-terminal Strep-TagII sequence and purified on Strep-Tactin columns (IBA Lifesciences*).

TCR cDNA for the α and β chain of insulin-reactive T cell hybridoma and primary cells were subcloned into the fly expression vector pRMHa3 or pMT/Bip/V5-His (Invitrogen*) and sequenced. The final constructs code for the VαCα and the VβCβ chains, respectively, followed by a linker sequence (SSADL), a thrombin site (LVPRGS), a leucine zipper (acidic for the α chain, basic for the β chain) and a hexahistidine tag. Vectors were co-transfected into SC2 cells along with a vector encoding a puromycin-resistance gene and stable cell-lines were established. Soluble TCRs were purified from culture supernatants, as previously described (55).

Peptides.

Synthetic peptides, HEL_{11-27} (AMKRHGLDNYRGYSLGN), Ins_{12-20} (TEGVEALYLVCGGGS), and Ins_{13-21} (TEGEALYLVCGEGGS) in which N- and C-termini were extended by TEG- and GGS- sequences, respectively(39), Ins_{9-23} (SHLVEALYLVCGERG) were ≥ 95% pure and synthesized by AnaSpec Inc*.

Site-directed mutagenesis.

PCR site-directed mutagenesis was carried out using the QuickChange II PfuUltra High-Fidelity DNA Polymerase (Agilent*) and verified by DNA sequencing.

Islet isolation and cell preparation

Islets were isolated using a modified protocol derived from Li(56). Briefly, pancreata were isolated and incubated for 60 min at 37°C after injection of collagenase P through the common bile duct. After several washes, islets were isolated on a metal strainer and hand-

picked under a dissection microscope. An average of 200-300 islets were obtained per mouse. For making single cell suspension, islets were digested with trypsin or dispase at 37°C and washed extensively before being counted.

Cell preparation, Cell Staining and Flow Cytometry Analysis.

Non-islet single cell suspensions were prepared by mechanical disruption of the corresponding organs in HBSS buffer and erythrocytes were removed by osmotic lysis. Cells were washed with FACS buffer (PBS containing 3% FCS and 0.05% NaN_3) and incubated with 0.5 mg/ml of avidin (Sigma) and Fc block (BD Biosciences) in FACS buffer for 1 h at RT. Cells were then washed once and stained with PE-labeled or PE-Cyanine 7 labeled MHC/peptide tetramers at a final concentration of 10 mg/ml in FACS buffer for 1 h at RT. For co-staining of surface markers FITC-anti-CD4 (clone RM4-4, BD Biosciences*), Allophycocyanin-anti-B220 (clone RA3-6B2, eBioscience*) and Allophycocyanin-anti-CD8 (clone 53-6.7, eBioscience*) were used. Exclusion of dead cells was done by propidium iodide labeling (Invitrogen*). Flow cytometry was performed using a FACS LSR-II instrument (Becton Dickinson*) or a MACSQuant Analyzer (Miltenyi Biotec*) and the data analyzed using FlowJo software (TreeStar Inc.*). Staining of T cell hybridomas with MHC tetramers was carried out in the same way.

CD4 T cell Responses.

For plate-bound activation assays, pMHC were coated overnight in PBS at 4°C at various concentration in flat-bottom 96 well plates, and washed twice in PBS before plating 4×10^4 hybridoma T cells per well. After 24h incubation at 37°C, supernatants were harvested and assayed for IL2 content using a radioactive IL2-dependent NK cell line bioassay.

For assays with live antigen presenting cells (APCs), T cell hybridomas were incubated with 1×10^5 APCs per well and increasing concentration of peptides.

All assays were performed using biological triplicates and performed in at least three independent experiments.

Single cell analysis.

For single cell analysis, T cells were sorted with pMHC tetramers on a FACSARIA III machine (BD Biosciences*) directly into RT buffer (10 μl per well). Protocols for preamplification and amplification for gene expression analysis and TCR sequencing have been detailed in recent publications(25). Gene expression analysis was performed on a Biomark unit with 96×96 Dynamic array IFCs, while sequencing was performed on an Access Array instrument using 48×48 Library Prep IFCs (Fluidigm*). Gene expression data quality control was performed using the Fluidigm software package and manual inspection of each melting curve to remove cells in which primer dimers were interfering with signal. Post-curation, the data was analyzed with a home-made R-package (see below). DNA sequencing was performed on a MiSeq instrument (Illumina*). After stitching, TCR sequences were confronted to the IMGT database to determine TRAV and TRBV assignment(57). The following list of TRAV (x-axis) and TRBV (y-axis) segments appears in Figure 4: TRAV2, TRAV4-2, TRAV5-1, TRAV5D-4, TRAV6-1, TRAV6-2, TRAV6-3,

TRAV6-5, TRAV6-6, TRAV6D-4, TRAV6D-7, TRAV7-2, TRAV7D-2, TRAV7D-4, TRAV7N-4, TRAV8-1, TRAV8D-2, TRAV9-1, TRAV9-3, TRAV9D-3, TRAV9D-4, TRAV10, TRAV10D, TRAV11, TRAV12-1, TRAV12-2, TRAV14D-2, TRAV14D-3/DV8, TRAV16, TRAV16D/DV11, TRAV21/DV12, and TRBV1 TRBV2 TRBV5 TRBV12-2 TRBV13-1 TRBV13-2 TRBV13-3 TRBV14 TRBV15 TRBV16 TRBV17 TRBV19 TRBV20 TRBV24 TRBV29 TRBV31.3.

Surface Plasmon Resonance.

A BIACORE T200 instrument was used to determine interactions between purified MHC/peptide complexes and TCR molecules. TCR were immobilized on lipid bilayers coated on L1 chips by capture of their histidine tag. Lipid bilayers were produced by fusion of liposomes on the hydrophobic surface. Phosphatidylcholine (PC), cholesterol (C), dioleoyl phosphatidylcholine (DOPC), L-α-phosphatidylethanolamine (PE), L-α-phosphatidylglycerol (PG), 1,2-dioleoyl-$_{sn}$-glycero-3-[(N-(5-amino-1-carboxypentyl)imidodiacetic acid)succinyl](DOGS-NTA) were all from Avanti Polar Lipids*, and liposomes composition was 60:20:5:5:10 (PC:C:DOPC:PE:PG:DOGS-NTA) weight ratio. Liposomes were produced by extrusion at 1mg.ml^{-1} in PBS on 400nm polycarbonate disks(58). Streptag modified pMHC molecules were injected over the surface after stabilization of baseline in filtered and degassed PBS at a flow rate of 20-30 μl/min. To avoid regeneration of the surface between injections, kinetics studies were performed using the single cycle mode using an irrelevant TCR in the subtraction flow cell. K_d values, as well as on- and off-rates, were obtained by non-linear curve fitting of subtracted curves using the 1:1 Langmuir binding model using the BIAevaluation program (version 3.0.2).

Statistics.

Fisher's exact test and Student's *t*-test (two-tailed) were used for statistical analyses.

R analysis methods

Single-cell expression data, in the form of qPCR C_t values from the Fluidigm Biomark HD system, were analyzed in the R programming environment according to recommendations from the Fluidigm Singular Analysis Toolset documentation. Log_2 expression values were calculated using the default Limit of Detection C_t value of 24, and negative log_2 expression values were set to zero. Log_2 expression values were then normalized per individual cell by dividing each cell's gene expression values by its Gapdh expression value. These normalized values were median-centered for further analysis.

The expression of 96 genes was quantified in 1746 individual cells. Cells were removed from the analysis if no expression of any gene was detected in the isolate (111 cells removed), or if Gapdh expression was markedly low (55 cells removed). Cells with relatively low total expression were filtered by clustering the cells and removing clusters with low cumulative normalized log_2 expression values (1131 cells removed).

Differential gene expression was calculated using the non-parametric Kruskal-Wallis test by ranks, due to the multimodal distributions of most genes. P-values were corrected by the Benjamini–Hochberg procedure.

The “Rtsne” R package was used for t-SNE dimensionality reduction. Violin, table, and t-SNE plots were created using the “ggplot2” R package(59). Heatmaps are based on the heatmap.2 function from the “gplots” R package. The columns of the heatmaps are ordered from lowest to highest differential expression p-values, and the rows are ordered by hierarchical clustering based on Euclidean distance.

Supplementary Material

Refer to Web version on PubMed Central for supplementary material.

ACKNOWLEDGMENTS

We acknowledge the outstanding support that the flow cytometry and DNA sequencing cores of Scripps Research and their personels provided to us throughout the performance of the current study.

Funding was provided by the National Institutes of Health Clinical and Translational Science Award issued to the Scripps Translational Science Institute UL1TR002550, TL1TR002551 to S.S. and L.G. and KL2TR001112 to B.A., and the National Institute of Health RO1DK058177 to E.U., R01DK099317 to M.N., RO1DK097605 and DK107541 to Y.C., and 1R01DK117138 to L.T. B.A was a resident of the Scripps Clinic & Green Hospital Internal Medicine Residency ABIM Research pathway during the course of the study.

Litterature cited

1. McDevitt HO, Bodmer WF, HL-A, immune-response genes, and disease. Lancet 1, 1269–1275 (1974). [PubMed: 4134154]
2. Nerup etal J., HL-A antigens and diabetes mellitus. Lancet2, 864–866 (1974). [PubMed: 4137711]
3. Polychronakos C, Li Q, Understanding type 1 diabetes through genetics: advances and prospects. Nat Rev Genet 12, 781–792 (2011). [PubMed: 22005987]
4. Todd JA, Etiology of type 1 diabetes. Immunity 32, 457–467 (2010). [PubMed: 20412756]
5. Aly TA et al., Extreme genetic risk for type 1A diabetes. Proceedings of the National Academy of Sciences of the United States of America 103, 14074–14079 (2006). [PubMed: 16966600]
6. Todd JA, Bell JI, McDevitt HO, HLA-DQ beta gene contributes to susceptibility and resistance to insulin-dependent diabetes mellitus. Nature 329, 599–604 (1987). [PubMed: 3309680]
7. Hu X et al., Additive and interaction effects at three amino acid positions in HLA-DQ and HLA-DR molecules drive type 1 diabetes risk. Nature genetics 47, 898–905 (2015). [PubMed: 26168013]
8. Corper AL et al., A structural framework for deciphering the link between I-Ag7 and autoimmune diabetes. Science (New York, N.Y288, 505–511 (2000).
9. Yoshida K et al., The diabetogenic mouse MHC class II molecule I-Ag7 is endowed with a switch that modulates TCR affinity. The Journal of clinical investigation 120, 1578–1590 (2010). [PubMed: 20407212]
10. Latek RR et al., Structural basis of peptide binding and presentation by the type I diabetes-associated MHC class II molecule of NOD mice. Immunity 12, 699–710 (2000). [PubMed: 10894169]
11. Suri A, Walters JJ, Gross ML, Unanue ER, Natural peptides selected by diabetogenic DQ8 and murine I-A(g7) molecules show common sequence specificity. The Journal of clinical investigation 115, 2268–2276 (2005). [PubMed: 16075062]
12. van Lummel M et al., Type 1 diabetes-associated HLA-DQ8 transdimer accommodates a unique peptide repertoire. J Biol Chem 287, 9514–9524 (2012). [PubMed: 22184118]
13. Scott CA, Peterson PA, Teyton L, Wilson IA, Crystal structures of two I-Ad-peptide complexes reveal that high affinity can be achieved without large anchor residues. Immunity 8, 319–329 (1998). [PubMed: 9529149]
14. Stratmann T et al., The I-Ag7 MHC class II molecule linked to murine diabetes is a promiscuous peptide binder. J Immunol 165, 3214–3225 (2000). [PubMed: 10975837]

15. Hovhannisyan Z et al., The role of HLA-DQ8 beta57 polymorphism in the antigluten T-cell response in coeliac disease. Nature 456, 534–538 (2008). [PubMed: 19037317]
16. Levisetti MG, Suri A, Petzold SJ, Unanue ER, The insulin-specific T cells of nonobese diabetic mice recognize a weak MHC-binding segment in more than one form. J Immunol 178, 6051–6057 (2007). [PubMed: 17475829]
17. Wan X et al., Pancreatic islets communicate with lymphoid tissues via exocytosis of insulin peptides. Nature, (2018).
18. Mallet-Designe VI et al., Detection of low-avidity CD4+ T cells using recombinant artificial APC: following the antiovalbumin immune response. J Immunol 170, 123–131 (2003). [PubMed: 12496391]
19. Landais E et al., New design of MHC class II tetramers to accommodate fundamental principles of antigen presentation. J Immunol 183, 7949–7957 (2009). [PubMed: 19923463]
20. Crawford F et al., Specificity and detection of insulin-reactive CD4+ T cells in type 1 diabetes in the nonobese diabetic (NOD) mouse. Proceedings of the National Academy of Sciences of the United States of America 108, 16729–16734 (2011). [PubMed: 21949373]
21. Stadinski BD et al., Diabetogenic T cells recognize insulin bound to IAg7 in an unexpected, weakly binding register. Proceedings of the National Academy of Sciences of the United States of America 107, 10978–10983 (2010). [PubMed: 20534455]
22. Mansiaux Y, Joseph AP, Gelly JC, de Brevern AG, Assignment of PolyProline II conformation and analysis of sequence--structure relationship. PLoS One 6, e18401 (2011). [PubMed: 21483785]
23. Mohan JF, Petzold SJ, Unanue ER, Register shifting of an insulin peptide-MHC complex allows diabetogenic T cells to escape thymic deletion. The Journal of experimental medicine 208, 2375–2383 (2011). [PubMed: 22065673]
24. Stratmann T et al., Susceptible MHC alleles, not background genes, select an autoimmune T cell reactivity. The Journal of clinical investigation 112, 902–914 (2003). [PubMed: 12975475]
25. Holt M et al., Gene Profiling and T Cell Receptor Sequencing from Antigen-Specific CD4 T Cells. Methods Mol Biol 1712, 217–238 (2018). [PubMed: 29224077]
26. Kalekar LA et al., CD4(+) T cell anergy prevents autoimmunity and generates regulatory T cell precursors. Nature immunology 17, 304–314 (2016). [PubMed: 26829766]
27. Mukherjee S, Maiti PK, Nandi D, Role of CD80, CD86, and CTlA4 on mouse CD4(+) T lymphocytes in enhancing cell-cycle progression and survival after activation with PmA and ionomycin. J Leukoc Biol 72, 921–931 (2002). [PubMed: 12429713]
28. Podojil JR, Miller SD, Cross-linking of CD80 on CD4+ T cells activates a calcium-dependent signaling pathway. J Immunol 182, 766–773 (2009). [PubMed: 19124719]
29. Dominguez CX et al., The transcription factors ZEB2 and T-bet cooperate to program cytotoxic T cell terminal differentiation in response to LCMV viral infection. The Journal of experimental medicine 212, 2041–2056 (2015). [PubMed: 26503446]
30. Holst J, Vignali KM, Burton AR, Vignali DA, Rapid analysis of T-cell selection in vivo using T cell-receptor retrogenic mice. Nat Methods 3, 191–197 (2006). [PubMed: 16489336]
31. Lund T et al., Prevention of insulin-dependent diabetes mellitus in non-obese diabetic mice by transgenes encoding modified I-A beta-chain or normal I-E alpha-chain. Nature 345, 727–729 (1990). [PubMed: 2163026]
32. Miyazaki T et al., Direct evidence for the contribution of the unique I-ANOD to the development of insulitis in non-obese diabetic mice. Nature 345, 722–724 (1990). [PubMed: 2113614]
33. Slattery RM et al., Prevention of diabetes in non-obese diabetic I-Ak transgenic mice. Nature 345, 724–726 (1990). [PubMed: 1972779]
34. Singer SM, Tisch R, Yang XD, McDevitt HO, An Abd transgene prevents diabetes in nonobese diabetic mice by inducing regulatory T cells. Proceedings of the National Academy of Sciences of the United States of America 90, 9566–9570 (1993). [PubMed: 8415742]
35. Quartey-Papafio R et al., Aspartate at position 57 of nonobese diabetic I-Ag7 beta-chain diminishes the spontaneous incidence of insulin-dependent diabetes mellitus. J Immunol 154, 5567–5575 (1995). [PubMed: 7730655]
36. Singer SM et al., Prevention of diabetes in NOD mice by a mutated I-Ab transgene. Diabetes 47, 1570–1577 (1998). [PubMed: 9753294]

37. Chen YG, Mathews CE, Driver JP, The Role of NOD Mice in Type 1 Diabetes Research: Lessons from the Past and Recommendations for the Future. Front Endocrinol (Lausanne) 9, 51 (2018). [PubMed: 29527189]
38. Robertson JM, Jensen PE, Evavold BD, DO11.10 and OT-II T cells recognize a C-terminal ovalbumin 323–339 epitope. J Immunol 164, 4706–4712 (2000). [PubMed: 10779776]
39. Mohan JF, Calderon B, Anderson MS, Unanue ER, Pathogenic CD4(+) T cells recognizing an unstable peptide of insulin are directly recruited into islets bypassing local lymph nodes. The Journal of experimental medicine 210, 2403–2414 (2013). [PubMed: 24127484]
40. Fousteri G et al., Subcutaneous insulin B:9–23/IFA immunisation induces Tregs that control late-stage prediabetes in NOD mice through IL-10 and IFNgamma. Diabetologia 53, 1958–1970 (2010). [PubMed: 20490452]
41. Levisetti MG, Suri A, Frederick K, Unanue ER, Absence of lymph nodes in NOD mice treated with lymphotoxin-beta receptor immunoglobulin protects from diabetes. Diabetes 53, 3115–3119 (2004). [PubMed: 15561941]
42. Fischer HJ et al., The Insulin Receptor Plays a Critical Role in T Cell Function and Adaptive Immunity. J Immunol 198, 1910–1920 (2017). [PubMed: 28115529]
43. Ferris ST et al., The islet-resident macrophage is in an inflammatory state and senses microbial products in blood. The Journal of experimental medicine 214, 2369–2385 (2017). [PubMed: 28630088]
44. Carrero JA et al., Resident macrophages of pancreatic islets have a seminal role in the initiation of autoimmune diabetes of NOD mice. Proceedings of the National Academy of Sciences of the United States of America 114, E10418–E10427 (2017). [PubMed: 29133420]
45. Pujol-Borrell R et al., HLA class II induction in human islet cells by interferon-gamma plus tumour necrosis factor or lymphotoxin. Nature 326, 304–306 (1987). [PubMed: 3102976]
46. Francisco LM et al., PD-L1 regulates the development, maintenance, and function of induced regulatory T cells. The Journal of experimental medicine 206, 3015–3029 (2009). [PubMed: 20008522]
47. Tan TG, Mathis D, Benoist C, Singular role for T-BET+CXCR3+ regulatory T cells in protection from autoimmune diabetes. Proceedings of the National Academy of Sciences of the United States of America 113, 14103–14108 (2016). [PubMed: 27872297]
48. Sprouse ML et al., High self-reactivity drives T-bet and potentiates Treg function in tissue-specific autoimmunity. JCI Insight 3, (2018).
49. Nakayama M et al., Prime role for an insulin epitope in the development of type 1 diabetes in NOD mice. Nature 435, 220–223 (2005). [PubMed: 15889095]
50. So M et al., Proinsulin C-peptide is an autoantigen in people with type 1 diabetes. Proceedings of the National Academy of Sciences of the United States of America 115, 10732–10737 (2018). [PubMed: 30275329]
51. Levisetti MG, Lewis DM, Suri A, Unanue ER, Weak proinsulin peptide-major histocompatibility complexes are targeted in autoimmune diabetes in mice. Diabetes 57, 1852–1860 (2008). [PubMed: 18398138]
52. Halbout P, Briand JP, Becourt C, Muller S, Boitard C, T cell response to preproinsulin I and II in the nonobese diabetic mouse. J Immunol 169, 2436–2443 (2002). [PubMed: 12193712]
53. Pathiraja V et al., Proinsulin-specific, HLA-DQ8, and HLA-DQ8-transdimer-restricted CD4+ T cells infiltrate islets in type 1 diabetes. Diabetes 64, 172–182 (2015). [PubMed: 25157096]
54. Scott CA, Garcia KC, Carbone FR, Wilson IA, Teyton L, Role of chain pairing for the production of functional soluble IA major histocompatibility complex class II molecules. The Journal of experimental medicine 183, 2087–2095 (1996). [PubMed: 8642319]
55. Garcia KC et al., Alphabeta T cell receptor interactions with syngeneic and allogeneic ligands: affinity measurements and crystallization. Proceedings of the National Academy of Sciences of the United States of America 94, 13838–13843 (1997). [PubMed: 9391114]
56. Li DS, Yuan YH, Tu HJ, Liang QL, Dai LJ, A protocol for islet isolation from mouse pancreas. Nat Protoc 4, 1649–1652 (2009). [PubMed: 19876025]
57. Lefranc MP, IMGT, the international ImMunoGeneTics database. Nucleic Acids Res 31, 307–310 (2003). [PubMed: 12520009]

58. Celia H, Wilson-Kubalek E, Milligan RA, Teyton L, Structure and function of a membrane-bound murine MHC class I molecule. Proceedings of the National Academy of Sciences of the United States of America 96, 5634–5639 (1999). [PubMed: 10318936]

59. Wickham H, ggplot2 : elegant graphics for data analysis Use R! (Springer, New York ; London, 2009), pp. viii, 212 p.

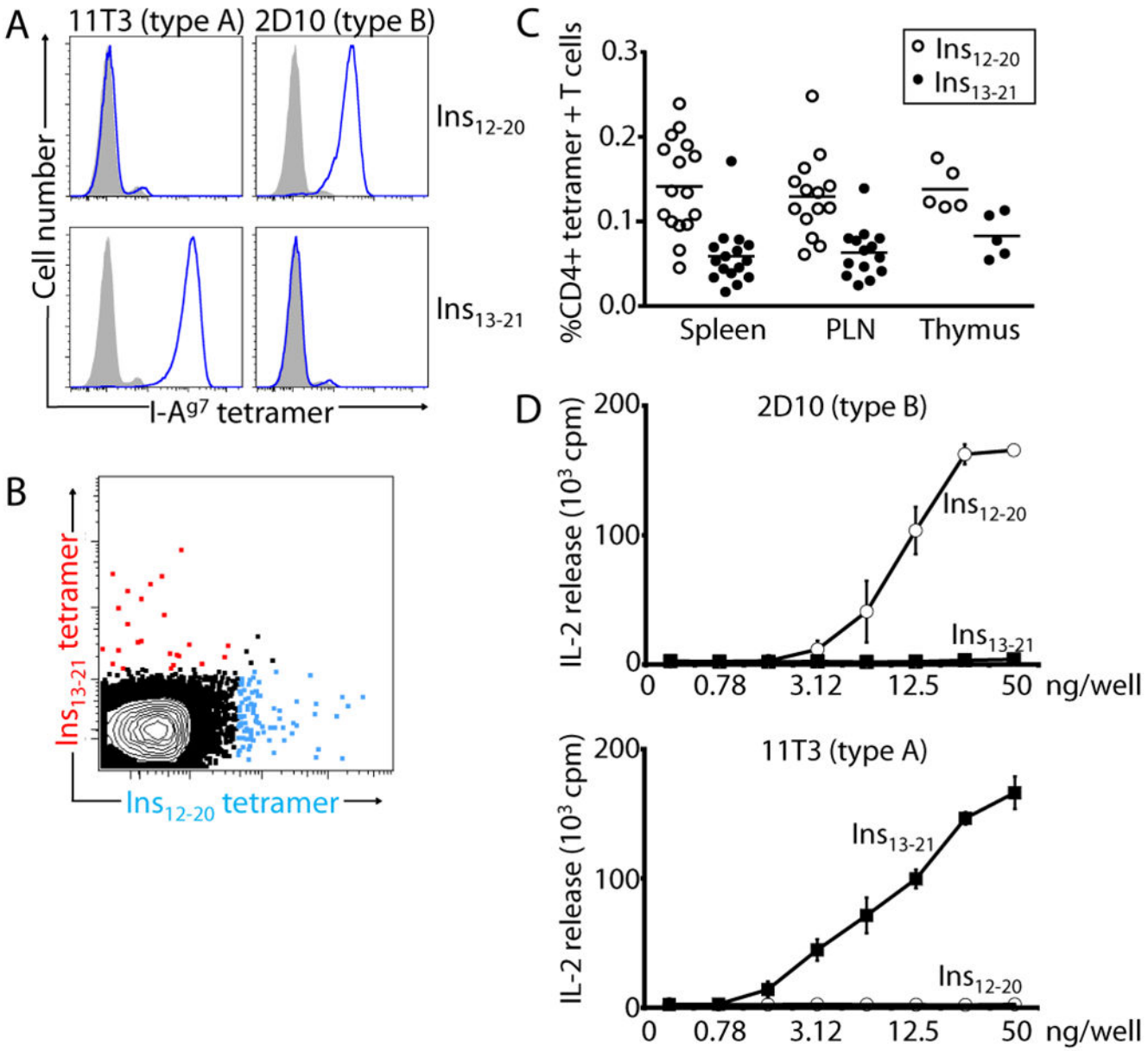

Figure 1: Characterization of insulin peptide-I-A^{g7} tetramers, and detection of register-specific CD4 cells in NOD mice.

A: specific staining of type A (Ins_{13-21} peptide) and type B (Ins_{12-20} peptide) anti-insulin T cell hybridomas of which 2D10 and 11T3 are representative members, respectively. B: Double stain of NOD mouse splenocytes with Ins_{12-20} (blue) and Ins_{13-21} peptide (red). Gating in on CD3+CD4+ (CD8-B220-CD11b)- population. C: Enumeration of Ins_{12-20} and Ins_{13-21} specific CD4+ T cells in spleen, PLNs, and thymi of 8 week old female NOD mice using register-specific tetramers. D: Register-specific activation of type A and B hybridoma T cells using recombinant I-A^{g7}-peptide coated wells. This result is representative of a minimum of 5 similar experiments. Each point is a biological triplicate (SD are represented for each triplicate).

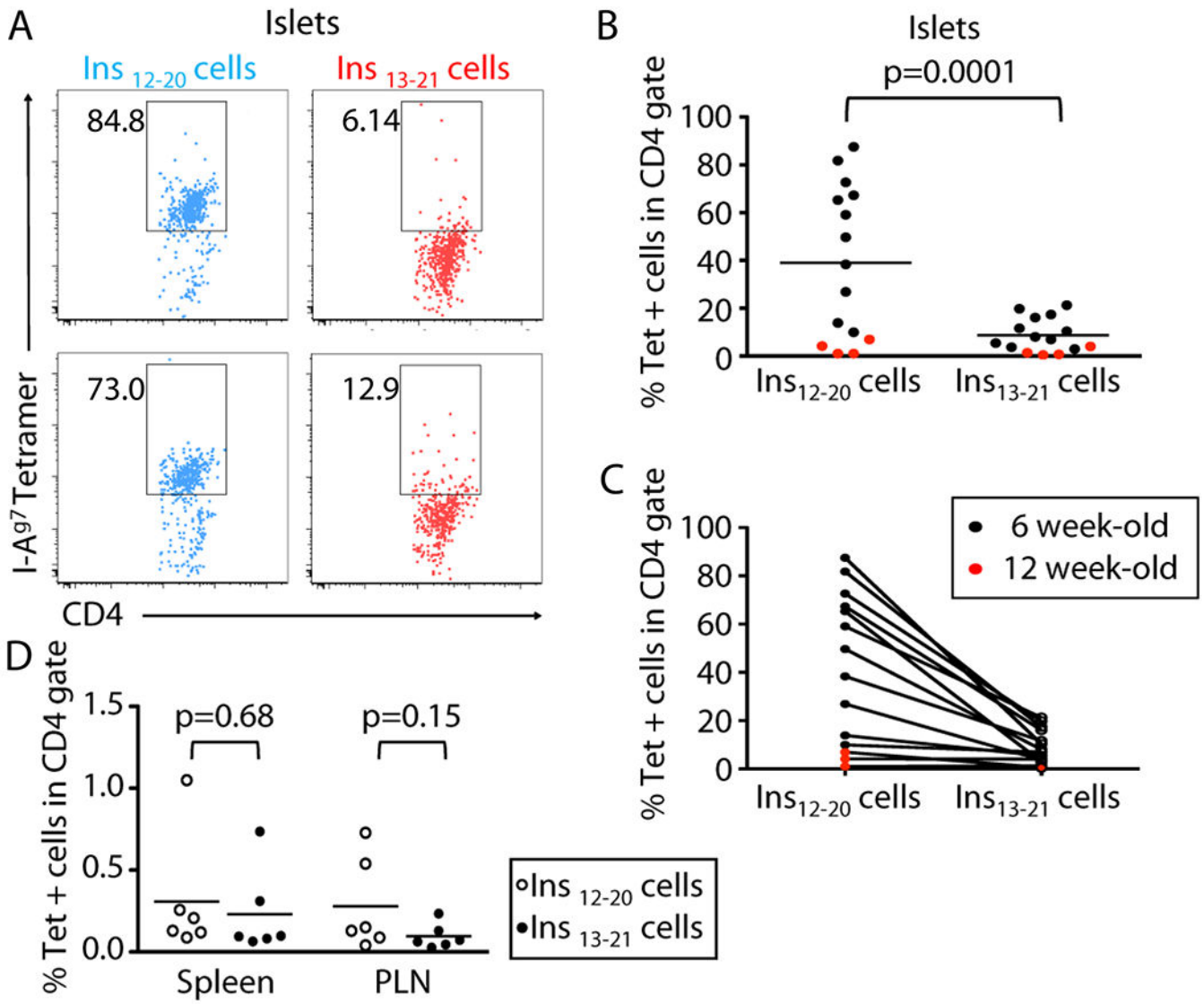

Figure 2: Anti-insulin register-specific populations dynamics in the islets during the course of disease in female NOD mice.

A: Two representative examples of $Ins_{12\text{-}20}$ and $Ins_{13\text{-}21}$ tetramer staining of islet-infiltrating CD4 T cells at 6 weeks of age. Numbers are percentage of total CD3+CD4+ cells. B, C: Representation of the percentages of $Ins_{12\text{-}20}$ and $Ins_{13\text{-}21}$ tetramer+ cells in the purified islets of eleven 6-week old and four 12-week old animals used in this study. While B shows numbers and mean value for all mice, C shows the pairwise analysis of both tetramers in each mouse. D: Percentage of $Ins_{12\text{-}20}$ and $Ins_{13\text{-}21}$ tetramer+ cells in spleen and PLNs of mice with established diabetes (20 weeks). Number could not be obtained from islets as most were destroyed. P values were calculated using an unpaired t-test two-tailed in PRISM.

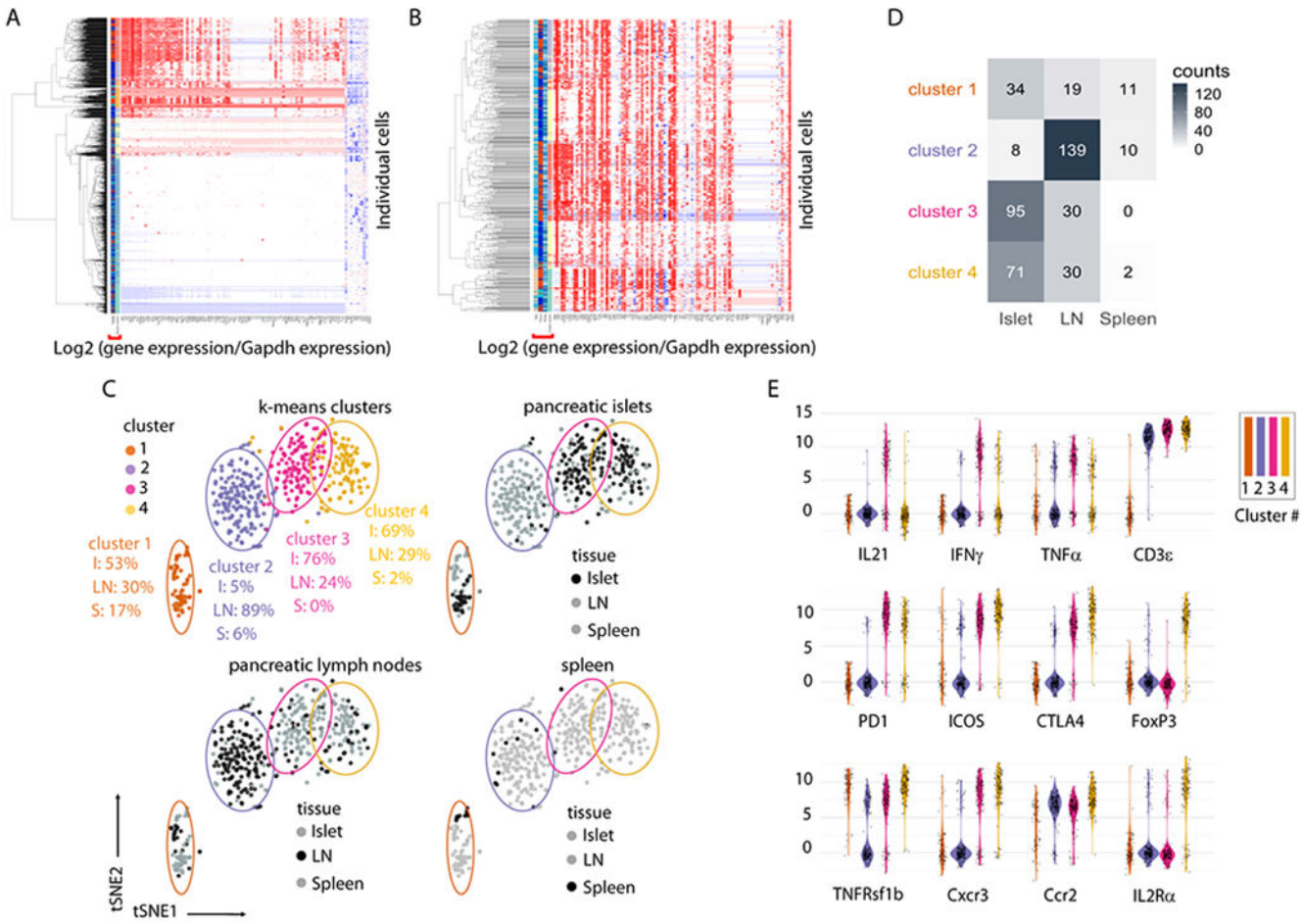

Figure 3: Single cell transcriptomics analysis of Ins_{12-20} and Ins_{13-21} tetramer+ cells sorted from spleen, PLNs and infiltrated islets.

Single tetramer+ CD4 T cells were sorted on a FACSAria instrument directly in RT buffer and examined for expression of a panel of 96 genes. A, B: heatmaps of all cells from all organs before (A), and after (B) removal of cells expressing low levels of >80% of all genes. C: T-distributed stochastic neighbor embedding (t-sne) analysis of the single cell gene expression data. The unsupervised cluster distribution (k-means) defined four separate groups of cells (upper left, group 1, brown, group 2, blue, group 3, red, group 4, yellow). The distribution of each group in islet (I), pancreatic lymph nodes (LN), and spleen (S) is indicated under each cluster. The other three panels show in black the representation of the cells from each tissue, pancreatic islets, pancreatic lymph nodes, and spleen, within each of the the four clusters, while cells from the other tissues are in grey. D: Heatmap of the representation of each cluster in all three tissues examined and represented in C. E: Violin plot representation of the 12 statistically most differentially expressed genes that defined clusters 1-4.

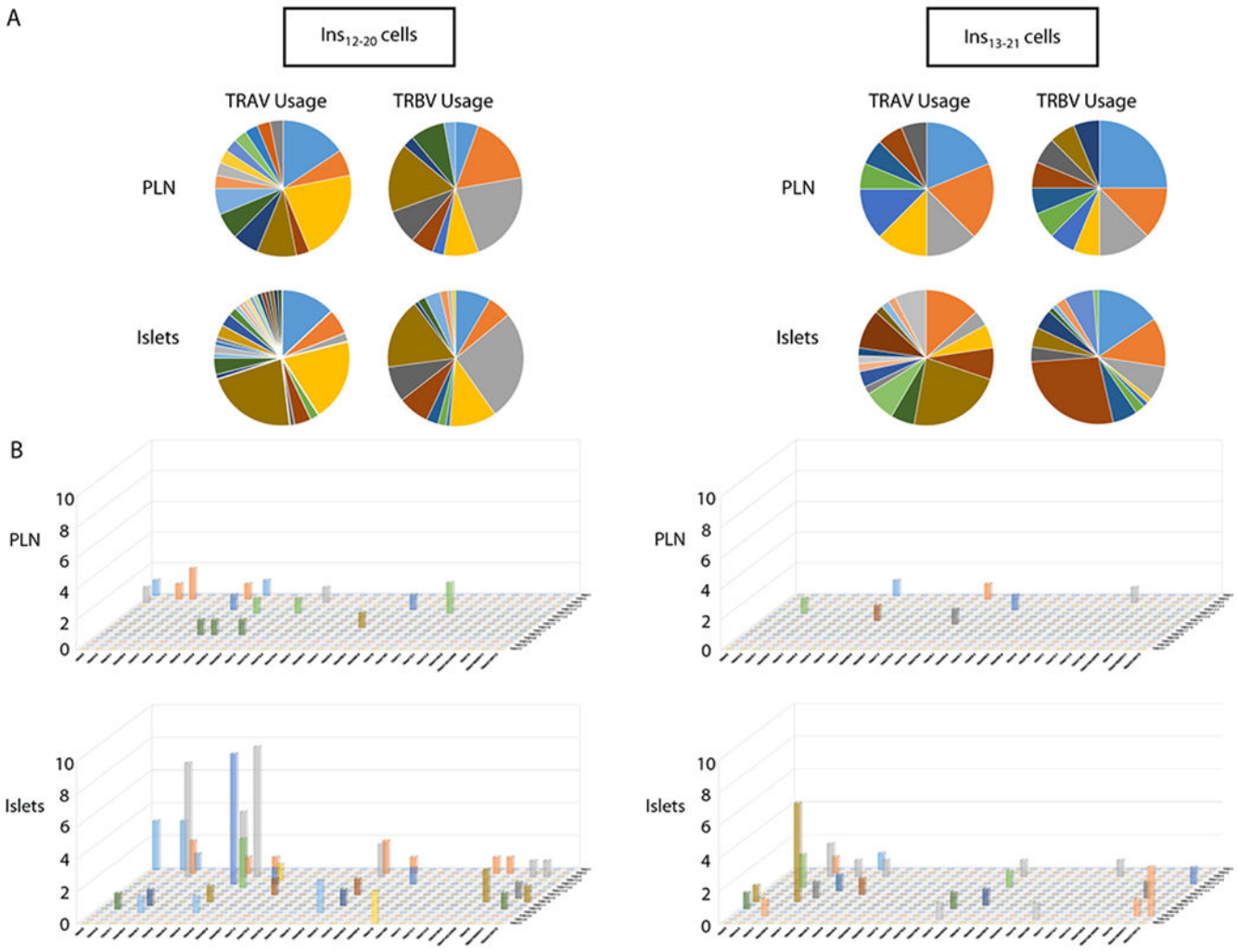

Figure 4: Single cell TCR αβ paired sequencing in PLNs and islets.

A: TRAV and TRBV usage in PLNs and islets for $Ins_{12\text{-}20}$ and $Ins_{13\text{-}21}$ tetramer+ cells. B: Clonal distribution of αβ TCR pairs in PLN and islets for $Ins_{12\text{-}20}$ and $Ins_{13\text{-}21}$ tetramer+ cells. The x axis lists the various TRAV segments, the z axis lists the TRBV segments (see material and methods for list), and the y axis indicates the number of cells for each TCR αβ pair. Numbers of sequences: islets $Ins_{12\text{-}20}$, 107 cells, PLN $Ins_{12\text{-}20}$, 36 cells, islets $Ins_{13\text{-}21}$, 84 cells, PLN $Ins_{13\text{-}21}$, 16 cells.

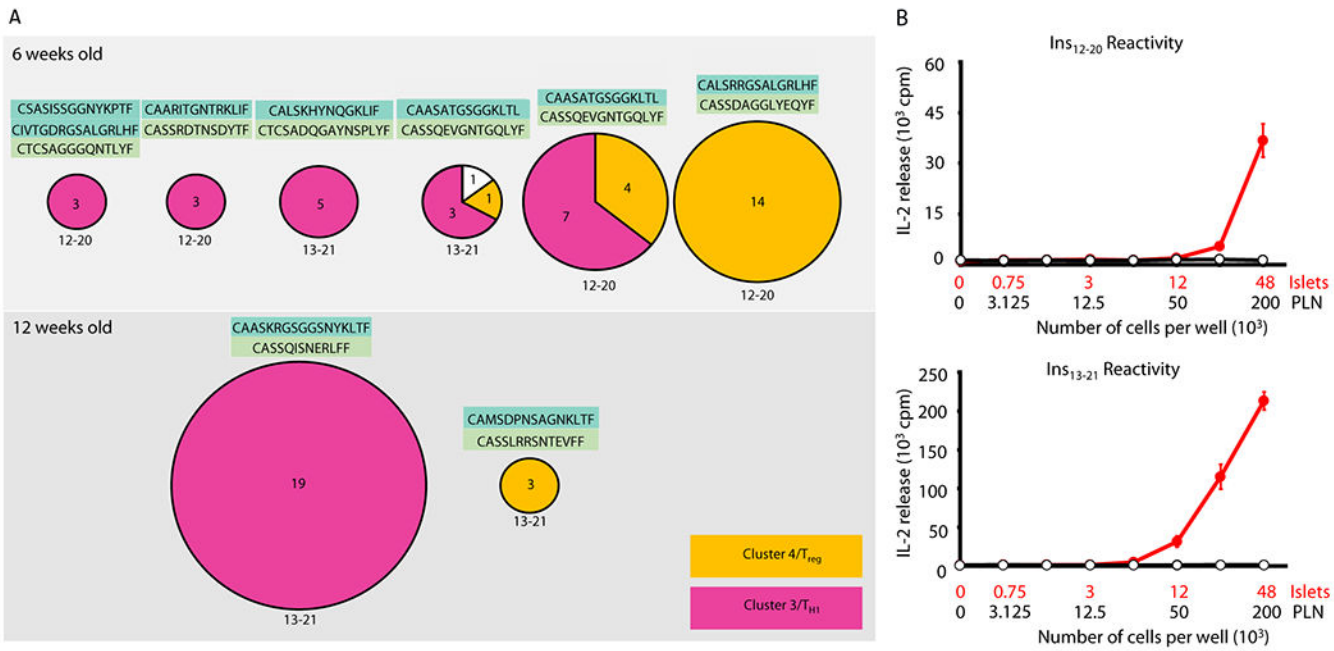

Figure 5: Analysis of the clonal expansion of anti-insulin CD4+ cells in the islets.

A: Clone CDR3α and CDR3β sequences are shown next to each circle. Each circle size is proportional to the clone size. Antigen specificity, Ins_{12-20} versus Ins_{13-21} is shown underneath each circle, while the cluster affiliation is represented in color (red for cluster 3, yellow for cluster 4). B: The islet clonal expansion correlated with the ability of fresh islet cells to stimulate Ins_{12-20} and Ins_{13-21}-specific T cell hybridomas (red line) in the absence of peptide addition, while PLN cells could not. Islet and PLN cell numbers are indicated. This experiment is representative of 5 similar experiments. Each dilution of cells was tested in triplicates and SD are shown.

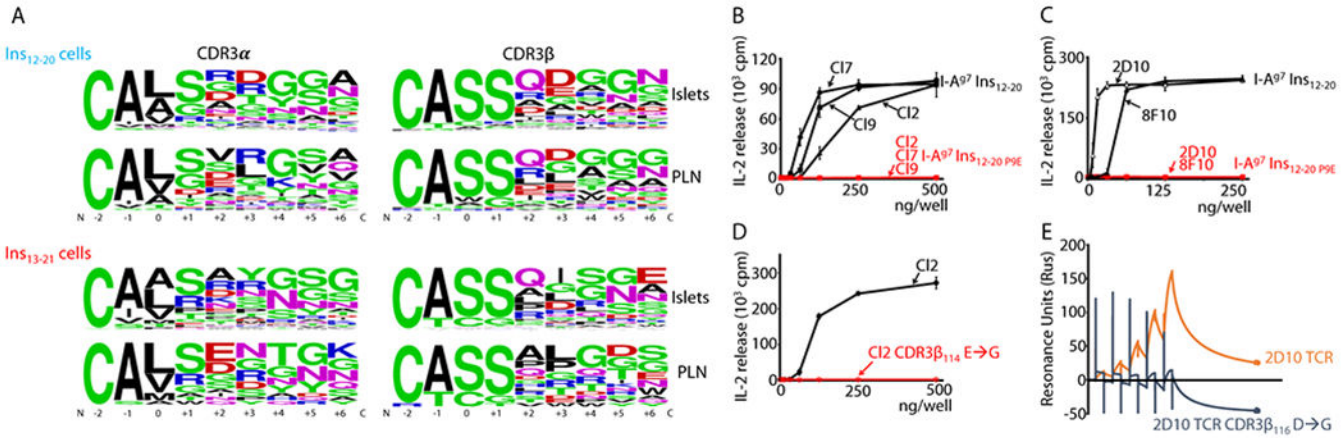

Figure 6: Ins_{12-20}-specific CD4+ T cells use a P9 switch for activation.

A: Analysis of CDR3 α and β sequences of Ins_{12-20} and Ins_{13-21} specific cells in both PLNs and islets. Schematic representation of the percentage of each amino acid at each position of the N-terminus of each CDR3, normalized against the frequency of each residue at each position. Numbering of the CDR3 residues follows the nomenclature of our previous publication(9, 15). B, C: Usage of the switch by Ins_{12-20} T cell clones. Clones 2, 7, and 9 isolated from islets (B), as well as 2D10 and 8F10 isolated after immunization (C) were tested for IL-2 release after stimulation on coated recombinant p-I-A^{g7} molecules retaining either the native peptide (black) or mutant P9E version (red). D: The effects of the mutation 114➔G in the CDR3β of TCR are shown for clone 2 using recombinant I-A^{g7}-Ins_{12-20} coated wells. WT hybridoma is in black, mutant in red. E: Direct surface plasmon resonance (SPR) measurements of the loss of affinity of recombinant 2D10 TCR after mutation D➔G at position 116 of the CDR3 β WT (red trace) and mutant (blue trace) TCRs were captured on lipid bilayers using DOGS lipids on a L1 chip and two-fold dilutions of recombinant I-A^{g7} Ins_{12-20} streptag were injected onto the surface using an irrelevant TCR in the flow cell used for subtraction. All functional experiments are representative of a minimum of 3 independent repeats. SPR measurements were performed twice.

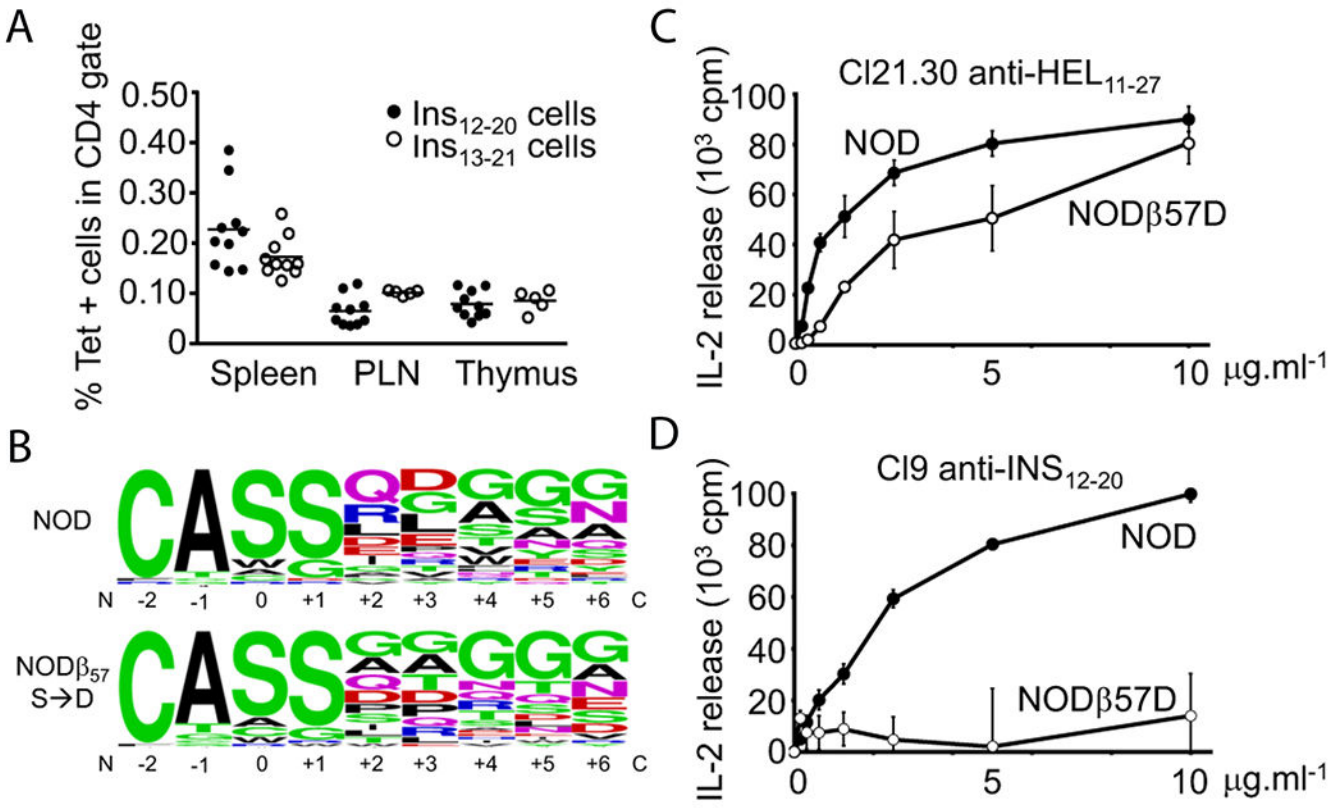

Figure 7: The in vivo substitution of serine β57 of I-A^{g7} for an aspartic acid modifies the anti-insulin T cell repertoire, and eliminates the switch in the anti-Ins$_{12-20}$ T cell population.

A: I-A$^{g7}_{57}$ S➔D Ins$_{12-20}$ and Ins$_{13-21}$ tetramers were used to enumerate register specific cells in the spleen and PLNs of NODβ$_{57}$➔D mutant animals. Numbers are expressed as percentages of CD3+CD4+ cells. B: The TCR repertoire of Ins$_{12-20}$-specific cells isolated from the PLNs of NOD and NODβ$_{57}$S➔D animals was examined. The sequences of the respective CDR3β are presented. C: The usage of the switch for TCR carrying a D/E residue in CDR3β was tested for hen egg lysozyme using T cell clone 21-30, and the long Ins$_{9-23}$ peptide using clone 9 using either NOD (black symbols) or NODβ$_{57}$S➔D (empty symbols) splenocytes as antigen presenting cells. The same experiment was repeated three times with similar results.

Table 1:

Differential gene expression between the four clusters defined by t-sne analysis of the single cell analysis (p values are indicated next to the name of each gene).

	Cluster 1	Cluster 2	Cluster 3	Cluster 4
1	Cd86 8.24e-35	Ccr7 3.42e-30	Pd1 2.57e-30	Foxp3 2.01e-36
2	Zeb2 2.31e-30	Il.7r 1.12e-17	IL.21 2.15e-23	Ctla4 7.36e-33
3	Tnfrsf1a 8.54e-27	Ccr6 3.87e-12	Ifng 3.41e-22	Il.2ra 6.24e-24
4	Icam1 1.64e-26	Ifi44 1.23e-09	Tnf 1.18e-15	Tnfrsf1b 1.17e-21
5	Tgfbr2 3.15e-22	Cxcl10 1.65e-09	Stat4 1.26e-14	Icos 2.26e-21
6	Ifngr1 4.85e-22	Ifit3 2.98e-08	Cd3e 3.25e-13	Cxcr3 1.91e-19
7	Cd80 3.56e-20	Bcl2 4.61e-08	Cd28 4.28e-10	Ifngr1 1.38e-14
8	Ccr1 3.98e-20	Il.25 1.23e-06	Fyn 3.65e-09	Ccr2 1.93e-13
9	Vav1 4.47e-15	Cd3e 2.78e-05	Zap70 3.74e-09	Cd3e 2.85e-12
10	Cd40 1.18e-13		Jak2 6.08e-09	Tbx21 2.62e-11
11	Il.4ra 7.38e-12		Icos 1.04e-08	Ly6e 1.76e-10
12	Pten 1.26e-11		Cxcr3 2.88e-08	Zap70 3.55e-10
13	Tnfrsf1b 2.49e-11		Ctla4 5.87e-08	Ccr5 1.72e-09
14	14 Pparg 9.59e-11		14 Bcl6 1.30e-07	Cd28 2.75e-09
15	Cd4 1.58e-10		Cd4 8.42e-07	Il.10 7.28e-08
16	Hprt 7.23e-10			Fyn 7.34e-08
17	Mx1 6.89e-09			Nur77 2.06e-07
18	Socs3 7.56e-09			Ccr4 2.33e-07
19	Stat1 2.29e-08			Il.12rb 2.89e-07
20	Irf7 4.40e-08			Tnfaip3 6.97e-07
21	Ccr5 4.54e-08			Irf1 1.30e-06
22	Traf2 7.27e-08			Il.27r 2.19e-06
23	Il.27 3.38e-07			Pd1 1.70e-05
24	Aim2 4.03e-07			Icam1 2.90e-05
25	Gsk3b 4.84e-07			
26	Pdl.1 6.35e-07			
27	Rsad2 3.89e-06			
28	Il.12b 2.39e-05			